# A Study of CVD Growth Kinetics and Film Microstructure of Zirconium Dioxide from Zirconium Tetra-*tert*-Butoxide

David J. Burleson,† Jeffrey T. Roberts,*,† Wayne L. Gladfelter,† Stephen A. Campbell,‡ and Ryan C. Smith†

*Departments of Chemistry and Electrical and Computer Engineering, University of Minnesota, Minneapolis, Minnesota 55455*

*Received August 21, 2001. Revised Manuscript Received December 4, 2001*

The chemical vapor deposition (CVD) of polycrystalline zirconium dioxide ($ZrO_2$) from zirconium tetra-*tert*-butoxide {$Zr[OC(CH_3)_3]_4$} is described. The $ZrO_2$ films, which were deposited on Si(100), were characterized by scanning electron microscopy, ellipsometry, X-ray diffraction, Rutherford backscattering spectrometry, and Auger electron spectroscopy. Deposition was studied between 380 and 825 °C, and at precursor pressures between $4 \times 10^{-5}$ and $1 \times 10^{-4}$ Torr. Film microstructure depends on deposition temperature, with low temperatures (<420 °C) leading to the formation of nearly equi-axed grains, moderate temperatures (450−550 °C) producing oblate grains, and high temperatures (>700 °C) giving rise to triangular grains. Film density decreases with increasing deposition temperature. The kinetics for steady-state $ZrO_2$ growth were studied as functions of temperature and precursor pressure. Results were fit to a two-step kinetic model involving reversible precursor adsorption followed by irreversible decomposition to $ZrO_2$. The induction period ($t_i$) to growth was measured as a function of temperature for a single precursor pressure ($9.4 \times 10^{-5}$ Torr); $t_i$ decreases with temperature from 490 s at 381 °C to less than 1 s at 743 °C.

## Introduction

High dielectric constant metal oxides are of technological interest as potential replacements for $SiO_2$ as the gate dielectric in metal oxide semiconductor field-effect transistors (MOSFETs). A replacement material is needed because device miniaturization using current technologies will encounter an abrupt limit at $SiO_2$ thicknesses of ∼1.5 nm.[1] At that point, direct tunneling across the oxide barrier will lead to unacceptable leakage currents, and it will be necessary to replace $SiO_2$ with a higher dielectric constant material for which equivalent capacitances can be obtained with higher oxide thicknesses.

The group IV oxides represent an important class of potential replacement materials for $SiO_2$. For instance, $ZrO_2$ has a dielectric constant of approximately 20, five times that of $SiO_2$. Several compounds have been studied as chemical vapor deposition (CVD) precursors to $ZrO_2$.[2] Inorganic precursors include zirconium(IV) nitrate [$Zr(NO_3)_4$, ZN] and zirconium(IV) chloride ($ZrCl_4$). While ZN is potentially a true single-source precursor, CVD from $ZrCl_4$ requires an oxygen source, typically $O_2$ or $H_2O$.[3−5] Another problem with $ZrCl_4$ is that reasonable growth rates are obtained only at relatively high deposition temperatures (>800 °C). Among metal−organic precursors for $ZrO_2$ are the Zr(IV) compounds zirconium acetylacetonate [$Zr(C_5H_7O_2)_4$] and zirconium tetra-*tert*-butoxide [$Zr(OC(CH_3)_3]_4$, ZTB]. The acetylacetonate complex has a very low vapor pressure and must be heated to ∼200 °C if reasonable deposition rates are to be achieved.[6] ZTB, on the other hand, has a higher vapor pressure, and it undergoes smooth decomposition to $ZrO_2$ without an additional oxygen source at substrate temperatures as low as 300 °C.[7] At low deposition temperatures (<300 °C) and in the presence of water, ZTB decomposes by hydrolysis to form $ZrO_2$ and 2-methyl-2-propanol (eq 1), the latter product then dehydrating to 2-methylpropene (eq 2).[8,9]

$$Zr[OC(CH_3)_3]_4 + 2H_2O \rightarrow ZrO_2 + 4C(CH_3)_3OH \quad (1)$$

$$4C(CH_3)_3OH \rightarrow 4CH_2{=}C(CH_3)_2 + 4H_2O \quad (2)$$

The most thorough study of $ZrO_2$ deposition from ZTB yet to appear was made by Cameron and George, who

* To whom correspondence should be addressed. Tel: (612) 625-2363. Fax: (612) 626-7541. E-mail: roberts@chem.umn.edu.
† Department of Chemistry.
‡ Department of Electrical and Computer Engineering.

(1) Brar, B.; Wilk, G. D.; Seabaugh, A. C. *Appl. Phys. Lett.* **1996**, *69*, 2728.
(2) Smith, R. C.; Ma, T.; Hoilien, N.; Tsung, L. Y.; Bevan, M. J.; Colombo, L.; Roberts, J.; Campbell, S. A.; Gladfelter, W. L. *Adv. Mater. Opt. Electron.* **2000**, *10*, 105.
(3) Choi, J.-H.; Kim, H.-G.; Yoon, S.-G. *J. Mater. Sci.: Mater. Electron.* **1992**, *3*, 87.
(4) Yamane, H.; Hirai, T. *J. Mater. Sci. Lett.* **1987**, *6*, 1229.
(5) Smith, R. C.; Hoilien, N.; Taylor, C. J.; Ma, T.; Campbell, S. A.; Roberts, J.; Copel, M.; Buchanan, D. A.; Gribelyuk, M.; Gladfelter, W. L. *J. Electrochem. Soc.* **2000**, *147*, 3472.
(6) Desu, S. B.; Shi, T.; Kwok, C. K. *Structure, Composition and Properties of MOCVD ZrO2 Thin Films*; Besmann, T. M., Gallois, B. M., Eds.; Materials Research Society: Pittsburgh, 1990; Vol. 168, p 349.

10.1021/cm0107629 CCC: $22.00 
Published on Web 01/29/2002

investigated the kinetics and mechanism for deposition under static pressure conditions.[10] In the work, the CVD reactor was backfilled with ZTB to approximately 0.05 Torr, and the conductance of a pump was manually throttled to maintain constant pressure during deposition. Under these conditions, the deposition rate increased with temperature up to 450 °C, at which point CVD growth became flux limited. The temperature dependence of the growth rate suggested an activation barrier of ~125 kJ·mol$^{-1}$ for decomposition, and the flux-limited deposition rate implied a reactive sticking coefficient of $6.8 \times 10^{-5}$. Both 2-methylpropene and 2-methyl-2-propanol were observed by mass spectrometry during deposition. It was suggested that the former of these products results from $\beta$-H elimination of adsorbed *tert*-butoxy groups [$(CH_3)_3CO$] and that the latter is formed via reaction of adsorbed *tert*-butoxy with adsorbed OH. Finally, Cameron and George found that the $ZrO_2$ growth rate decreases with increasing temperature above 500 °C, at which temperature the level of carbon contamination in the films begins to increase rapidly. The reduction in growth rate above 500 °C was attributed either to poisoning of ZTB decomposition by adsorbed carbon or to rapid desorption of unreacted precursor.

In this work, we describe the steady-state growth kinetics and microstructures of $ZrO_2$ CVD films deposited on Si(100) at growth temperatures >300 °C. We also describe the temperature-dependent induction period for $ZrO_2$ film growth. Finally, we extend a previously developed kinetic model to account for $ZrO_2$ CVD from the metal−organic precursor ZTB. These experiments were carried out under conditions for which ZTB is constantly swept into a reactor that is continuously pumped by a turbomolecular pump. This allows for a constant precursor flux to the substrate during deposition and the rapid removal of all gas-phase reaction products.

## Experimental Section

Zirconium dioxide films were deposited by chemical vapor deposition (CVD) in an ultrahigh vacuum (UHV)-compatible CVD reactor of base pressure $5 \times 10^{-9}$ Torr.[11] Depositions were performed in the absence of carrier gas. The ZTB precursor was introduced into the reactor via a stainless steel variable leak valve. It was stored in a sealed glass tube and was sufficiently volatile at room temperature to not require heating during deposition.

All films were deposited onto 1 cm$^2$-area Si(100) growth substrates. Before being introduced into the reactor, substrate samples were cleaned according to a standard procedure, involving treatment first by a 4:1 $H_2SO_4/H_2O_2$ mixture and then by 5% HF.[12] The samples were mounted onto a molybdenum sample holder and transferred into the UHV reactor using a load-lock system. The substrates were heated by electron bombardment of the molybdenum susceptor. Immediately before a deposition, a substrate was heated to ~800 °C to desorb hydrogen and then cooled to the desired deposition temperature.

The substrate temperature and precursor pressure were monitored continuously during deposition to maintain stable growth conditions. Substrate temperatures were measured using an optical pyrometer (E2T Pulsar II) and are accurate to two significant figures, although three significant figures are used to describe growth conditions in this work. Precursor pressures were measured with a nude ion gauge (Granville-Philips 271). Precursor pressures were studied in the range between $4 \times 10^{-5}$ and $1 \times 10^{-4}$ Torr. Except for the induction period studies, deposition times ranged from 30 min to 2 h with a final thickness of approximately 2000 Å.

Films were characterized by scanning electron microscopy (SEM, Hitachi S-900), Rutherford backscattering spectrometry (RBS), X-ray diffraction (XRD, Siemans D-5005), Auger electron spectroscopy (AES, Φ 15−255G), and ellipsometry (Gaertner). The thicknesses of thin (<1000 Å) films were measured ellipsometrically. The X-ray diffractometer used a copper source anode operated at 1.8 kW, and a 5 keV accelerating voltage was utilized for the collection of SEM images. The thicknesses of thicker films were obtained from analysis of the cross-sectional SEM images. The digital images were transferred into Adobe Photoshop, where the total cross-sectional area of a film was measured in pixel units and then divided by the film width. The image scale bar was then used to convert between pixel and true length units. This method was especially useful for the analysis of rougher films grown at higher deposition temperatures. Grain sizes were calculated in a similar manner from the plan-view SEM images.

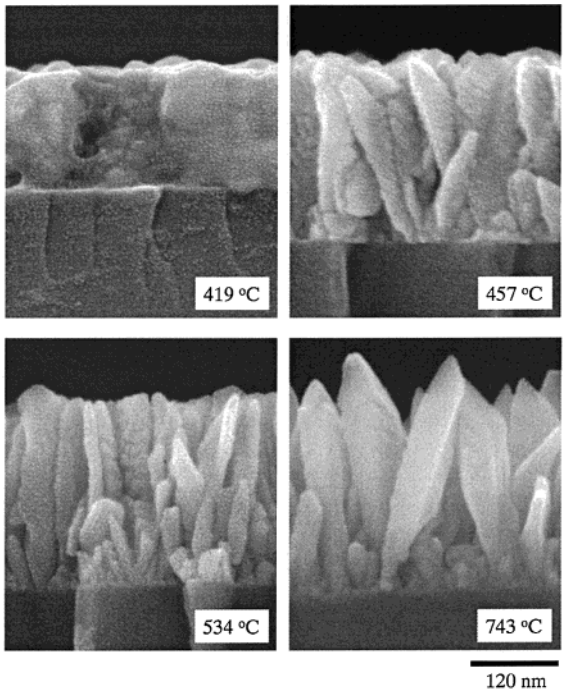


**Figure 1.** Cross-sectional SEM images of $ZrO_2$ films deposited from ZTB at 419, 457, 534, and 743 °C.

## Results

**Microstructure and Morphology.** Cross-sectional and plan-view SEM images of $ZrO_2$ films deposited from ZTB at 419, 457, 534, and 734 °C are shown in Figures 1 and 2, respectively. For low deposition temperatures (419 °C), the plan-view SEM images reveal a relatively dense microstructure, with $ZrO_2$ grains that have a slightly oval shape. Viewed from above, the average grain diameter is 70 nm. Cross-sectional images estab-

(7) Xue, Z.; Vaarstra, B. A.; Caulton, K. G.; Chisholm, M. H.; Jones, D. I. *Eur. J. Solid State Inorg. Chem.* **1992**, *29*, 213.
(8) Bradley, D. C. *Chem. Rev.* **1989**, *89*, 1317.
(9) Ritala, M.; Kukli, K.; Rahtu, A.; Raisanen, P. I.; Leskela, M.; Sajavaara, T.; Keinonen, J. *Science* **2000**, *288*, 319.
(10) Cameron, M. A.; George, S. M. *Thin Solid Films.* **1999**, *348*, 90.
(11) Chen, S.; Masen, M. G.; Gysling, H. J.; Paz-Pujalt, G. R.; Blanton, T. N.; Castro, T.; Chen, K. M.; Fictorie, C. P.; Gladfelter, W. L.; Franciosi, A.; Cohen, P. I.; Evans, J. F. *J. Vac. Sci. Technol., A* **1993**, *11*, 2419.
(12) Kim, H.-S. *J. Appl. Phys.* **1998**, *85*, 3278.

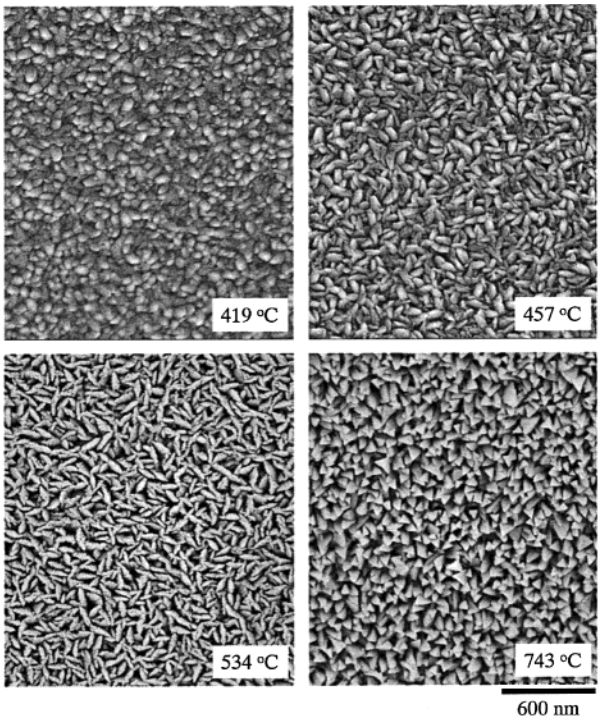


**Figure 2.** Plan-view SEM images of $ZrO_2$ films deposited from ZTB at 419, 457, 534, and 743 °C.

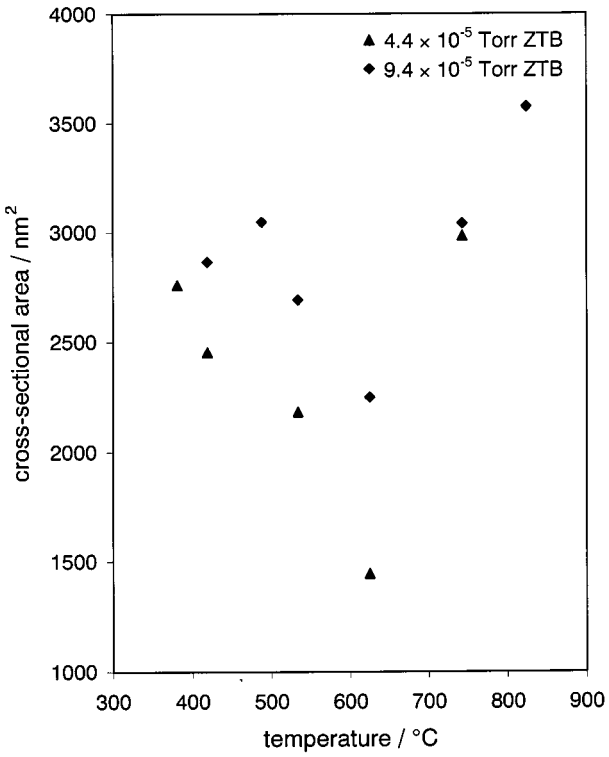


**Figure 3.** Plots of the mean cross-sectional area vs deposition temperature for ZTB pressures of $4.4 \times 10^{-5}$ and $9.4 \times 10^{-5}$ Torr.

lish that the grains extend the entire depth of the film and that they exhibit fully developed facets at the air−$ZrO_2$ interface. At slightly higher deposition temperatures (457 °C), the grains are more oblong, and the films appear to be less dense. Also, the films adopt a columnar structure, with grains that are on average perpendicular to the Si substrate. The trend toward lower density and more oblong-shaped grains is even more pronounced at 534 °C. The mean grain length and width, measured from above, are 100 and 40 nm, respectively, and there is a ridge-like structure along the grain edges. Between 534 and 743 °C, film microstructure undergoes a distinct change. The grains adopt triangular shapes and increase in size. Cross-sectional images show evidence of distinctly rougher films. Annealing a film grown below 534 °C at 775 °C for 30 min had no effect on film microstructure. Therefore, the microstructures are governed by events that occur during deposition.

Figure 3 shows how the mean cross-sectional area of a $ZrO_2$ grain depends on the deposition temperature. Mean grain sizes were obtained from the plan-view SEM grain area for 100 arbitrarily selected grains. The two sets of data refer to precursor pressures of $4.4 \times 10^{-5}$ and $9.4 \times 10^{-5}$ Torr. For both precursor pressures, there are two growth temperature regimes: one (below 625 °C) where mean grain size decreases with increasing temperature and another (above 625 °C) where size increases with temperature. Analogous behavior has also been observed in the CVD growth of $TiO_2$ from the precursors $Ti[OCH(CH_3)_2]_4$ and $Ti(NO_3)_4$.[13] Although analogous temperature-dependent trends are exhibited for the two data sets in Figure 3, films grown at $P_{ZTB} = 4.4 \times 10^{-5}$ have mean grain sizes that are on average 10% less than those grown at the same temperature for $P_{ZTB} = 9.4 \times 10^{-5}$.

The SEM images are from films deposited using a precursor pressure, $P_{ZTB}$, of $9.4 \times 10^{-5}$ Torr. Except for the average grain size being about 10% less, the microstructures of films deposited at $P_{ZTB} = 4.4 \times 10^{-5}$ Torr were not observably different from those shown in Figures 1 and 2.

Figure 4 shows how grain size *distribution* changes with deposition temperature, again for $P_{ZTB} = 4.4 \times 10^{-5}$ and $9.4 \times 10^{-5}$ Torr. The histograms in Figure 4 were generated by placing each grain of the above-described sample into a bin, depending on the grain's cross-sectional surface area. Bin 1 contained grains of area between 1 and 500 $nm^2$, bin 2 contained grains of area between 501 and 1000 $nm^2$, and so on. Films grown between 381 and 534 °C show a large distribution of grain sizes. Also, the distribution peak shifts toward smaller grain sizes as the deposition temperature increases. Films grown at 625 °C exhibit the smallest grain size and the narrowest distribution in grain size. Increasing the deposition temperature from 625 °C shifts the center of the grain size distribution to larger values and increases the size distribution.

XRD data of polycrystalline $ZrO_2$ films deposited at 381, 488, 625, 743, and 824 °C are shown in Figure 5. The presence of $ZrO_2$ diffraction peaks indicate at least partial crystallinity in all films, but the low signal-to-noise ratios for the lower temperature films suggest that an amorphous phase may also be present. The films exhibit some temperature-dependent preferred orientation, as indicated by the changing diffraction intensities of the monoclinic diffraction peaks, such as those for $2\theta = 24.50$ and 28.25°. Films deposited at 381 °C appear to be mostly tetragonal $ZrO_2$.[14] While tetragonal $ZrO_2$

(13) Taylor, C. J.; Gilmer, D. C.; Colombo, D. G.; Wilk, G. D.; Campbell, S. A.; Roberts, J.; Gladfelter, W. L. *J. Am. Chem. Soc.* **1999**, *121*, 5220.

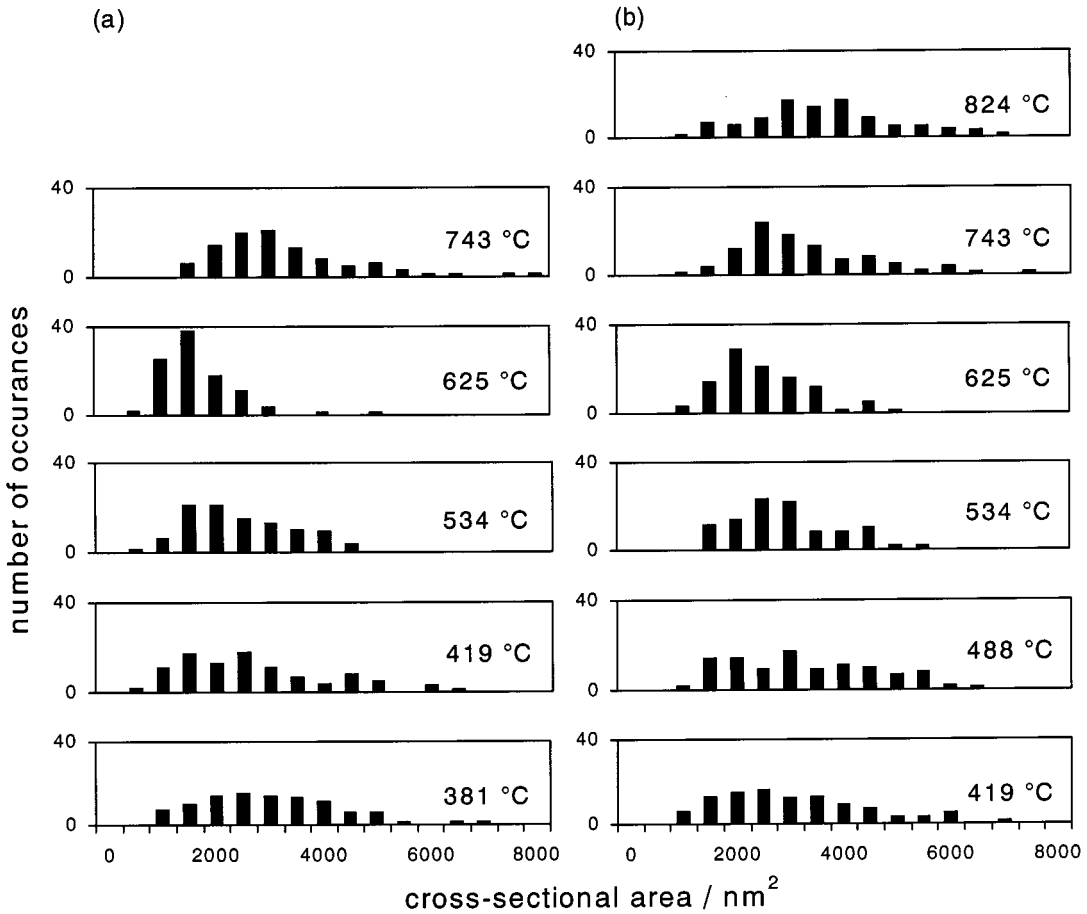


**Figure 4.** Histograms of the grain size distribution dependence on temperature for ZTB pressures of (a) $4.4 \times 10^{-5}$ and (b) $9.4 \times 10^{-5}$ Torr. The histogram bars represent the number of grains having a cross-sectional area within a bin range of 500 $nm^2$. Each full histogram is based on a sample size of 100 grains.

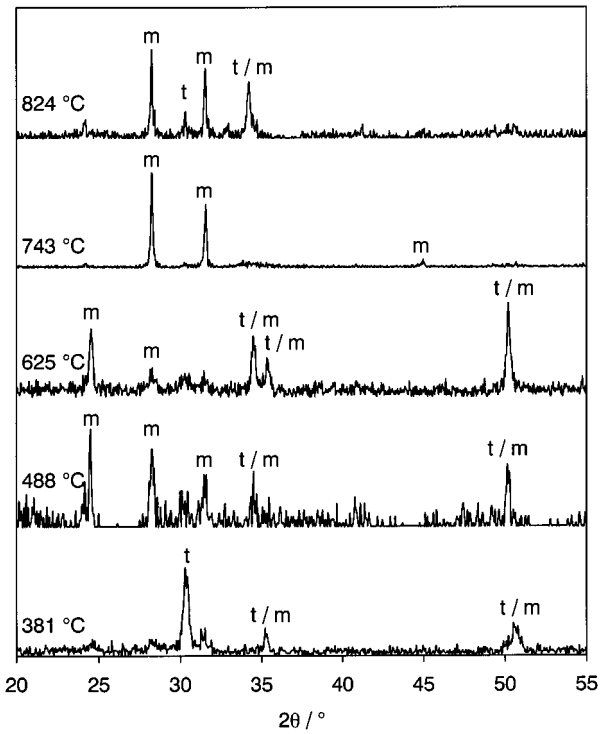


**Figure 5.** XRD of $ZrO_2$ films deposited from ZTB at 381, 488, 625, 743, and 824 °C. Reflections labeled m and t refer to the monoclinic and tetragonal phases, respectively.

is usually stable only between 1170 and 2370 °C, there are examples of metastable tetragonal $ZrO_2$ being formed at temperatures as low as room temperature.[15−19] Possible explanations for formation of the tetragonal phase include the formation of tetragonal nuclei which has a lower surface free energy than the monoclinic form and the existence of unpaired electrons resulting from oxygen vacancies.[20−25] By 488 °C, the films appear to deposit as monoclinic $ZrO_2$, although because of the similarities of the monoclinic and tetragonal diffraction patterns and because some of the reflections might not be observed due film texturing, some tetragonal $ZrO_2$ may still be present.[26] At higher temperatures, the increased signal-to-noise ratio implies that the films are more crystalline.

To determine the density of a film, the absolute amount of $ZrO_2$ in a film was measured using RBS. This

(14) Powder Diffraction File for *t*-ZrO2, International Center for Diffraction Data: Swarthmore, PA, Card # 17−0923.
(15) Claussen, N.; Kriven, W. M.; Ruhole, M. *J. Am. Ceram. Soc.* **1982**, *65*, 642.
(16) Wang, H.-C.; Lin, K.-L. *Mater. Sci. Eng., A* **1991**, *136*, 171.
(17) Farabaugh, E. N.; Feldman, A. *J. Vac. Sci. Technol., A* **1987**, *5*, 1671.
(18) Mitsuhashi, T.; Ichihara, M.; Tatsuke, U. *J. Am. Ceram. Soc.* **1974**, *57*, 97.
(19) Takahashi, Y.; Kawae, T.; Nasu, M. *J. Cryst. Growth* **1986**, *74*, 409.
(20) Garvie, R. C.; Goss, M. F. *J. Mater. Sci.* **1986**, *21*, 1253.
(21) Garvie, R. C. *J. Phys. Chem.* **1978**, *82*, 218.
(22) Zhan, Z.; Zeng, H. C. *J. Mater. Res.* **1998**, *12*, 2174.
(23) Garvie, R. C. *J. Phys. Chem.* **1965**, *69*, 1238.
(24) Wang, H.-C.; Lin, K.-L. *J. Mater. Sci.* **1991**, *26*, 2501.
(25) Osendi, M. I.; Moya, J. S. *J. Am. Ceram. Soc.* **1985**, *68*, 135.
(26) Powder Diffraction File for *m*-ZrO2, International Center for Diffraction Data: Swarthmore, PA, Card # 37−1484.

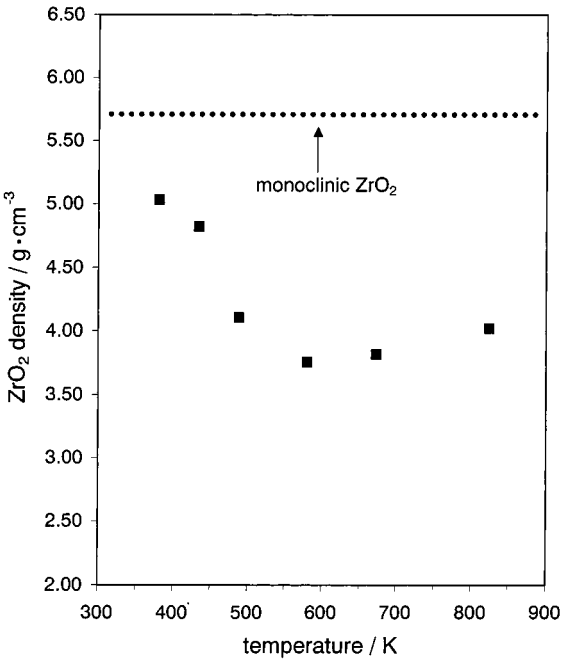


**Figure 6.** Temperature dependence of polycrystalline $ZrO_2$ density. The horizontal dotted line represents the density for single-crystal monoclinic $ZrO_2$.

was converted into an areal mass, which when divided by the SEM-determined film thickness yielded density. Figure 6 shows the calculated density values for seven polycrystalline $ZrO_2$ films that were deposited at $P_{ZTB} = 9.4 \times 10^{-5}$ with temperatures ranging from 381 to 824 °C. The horizontal dotted line represents the density of both amorphous and single-crystal monoclinic $ZrO_2$ (5.7 g·cm$^{-3}$).[27] There is a steady drop off in film density between deposition temperatures of 381 and 550 °C, followed by a slow increase above that temperature. Films grown at 381 °C have the highest density values, ~5 g·cm$^{-3}$, which is about 12% less than that of amorphous/single-crystal monoclinic $ZrO_2$. By 580 °C, the film has dropped to 3.8 g·cm$^{-3}$. Density increases slowly above this temperature to 4.0 g·cm$^{-3}$ at 824 °C.

Auger electron spectra recorded immediately after deposition reveal that films grown at temperatures ≤625 °C contain very little (≤0.5 mol %) carbon. However, carbon is present in films grown at higher temperatures, and the amount of carbon increases with temperature from 3.2% at 743 °C to 4.7% at 824 °C. These temperature-dependent trends are similar to those reported in a nonflow-CVD reactor using ZTB, although the amount of incorporated carbon in this work is lower.[10]

**Growth Kinetics.** Growth kinetics were studied in the following way: Two series of $ZrO_2$ films were deposited from ZTB at temperatures ranging from 381 to 824 °C; the two series corresponded to precursor pressures of $4.4 \times 10^{-5}$ and $9.4 \times 10^{-5}$ Torr. The deposition times were always sufficient to generate films that were ~2000 Å thick, as measured using cross-sectional SEM. The thickness of a film was then divided by the deposition time to yield the linear, steady-state growth rate. Growth rates were not corrected for the induction period because the induction period is always a small (<8%) fraction of the total deposition time (vide infra).

Figure 7a shows how the linear, steady-state growth rate of a $ZrO_2$ film depends on the deposition temperature. The growth rate data are plotted in an Arrhenius fashion, as the logarithm of the growth rate (in Å·min$^{-1}$) vs reciprocal temperature (in K). The growth rate plots show three distinct regimes. The first regime, which is operative at low temperatures (<500 °C for deposition pressures of $9.4 \times 10^{-5}$ Torr and <450 °C for $4.4 \times 10^{-5}$ Torr), shows an increase in the growth rate with increasing temperature. The second regime occurs at intermediate temperatures (500−675 °C for $9.4 \times 10^{-5}$ Torr and 450−675 °C for $4.4 \times 10^{-5}$ Torr). The deposition rate changes very little with temperature in this regime. Above 675 °C, the growth rate decreases as the temperature increases. These results are similar to those described by Cameron and George, in which three regimes for CVD growth were also identified.[10]

The induction period to steady-state growth was measured in the following way: A series of films were grown at constant precursor pressure and deposition temperature but with different deposition times. The thicknesses of the resulting films were then plotted vs deposition time. Figure 8 summarizes the results of three such sets of experiments: for $P_{ZTB} = 9.4 \times 10^{-5}$ Torr and temperatures of 381, 488, and 743 °C. A nonzero *x*-intercept indicates an induction period, the length of which decreases with increasing temperature, from 490 s at 381 °C to 190 s at 488 °C to 0 s at 743 °C. The slope is equal to the steady-state growth rate, and these values compare favorably to the linear growth rate data in Figure 7a. Note that the induction period is always <8% of the time required to deposit a 2000 Å film.

## Discussion

Zirconium dioxide films deposited at temperatures below ~400 °C have greater densities than those grown above 500 °C. The density differences are significant, with $\rho_{ZrO_2}^{400°C} \sim 5$ g·cm$^{-1}$ and $\rho_{ZrO_2}^{>500°C} \sim 3.8$ g·cm$^{-1}$. Because the density of tetragonal $ZrO_2$ (6.14 g·cm$^{-3}$ at 25 °C, based on unit cell dimensions) is greater than that of monoclinic (5.7 g·cm$^{-3}$), some of the change in density could be attributed to the tetragonal to monoclinic phase change observed between 381 and 488 °C in the deposited films.[28] However, the apparently large amorphous contents in films grown at 381 and 488 °C along with the plan-view and cross-sectional SEM images imply that most of the density change is due to increasingly inefficient grain packing. Above 734 °C, however, the film density no longer decreases with increasing temperature and may even increase slightly. This is probably due to the fact that the mean grain size begins to increase somewhere above 580 °C. This effect counteracts those of increasing intergrain distance and increasing film porosity.

The induction period decreases from 490 s at 381 °C to less than 1 s at 743 °C. Even for the lowest temperatures, the time required to grow a 2000 Å film is significantly longer than the induction period. Moreover,

(27) Lide, D. R. *Handbook of Chemistry and Physics*, 81st ed.; CRC Press: 2000.

(28) Amberg, M.; Gunter, J. R. *Solid State Ionics* **1996**, *84*, 313.

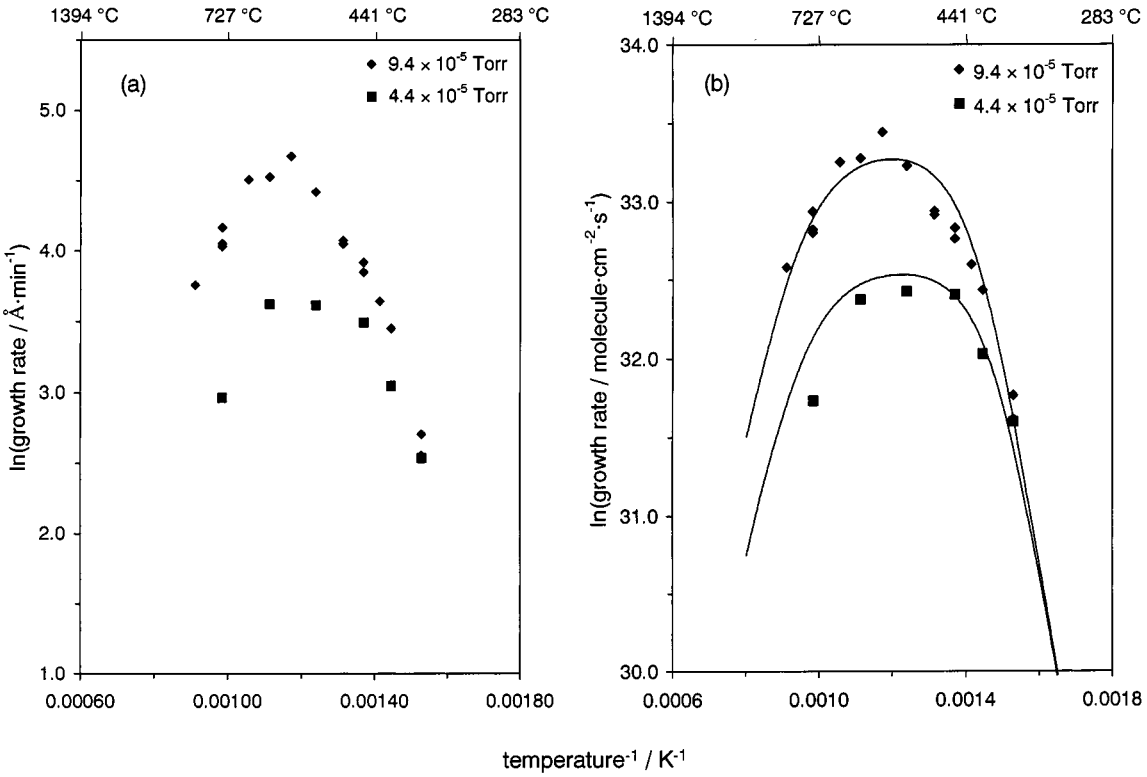


**Figure 7.** Temperature dependence of $ZrO_2$ growth rate for ZTB pressures of $4.4 \times 10^{-5}$ and $9.4 \times 10^{-5}$ Torr: (a) linear growth rate vs inverse temperature and (b) absolute growth rate vs inverse temperature. The solid lines are based on fits to the model described in the text.

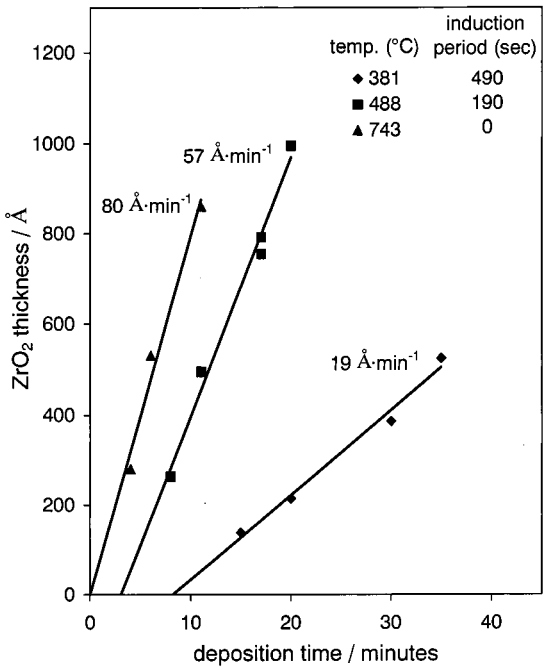


**Figure 8.** Plots of the film thickness vs deposition time at 381, 488, and 743 °C with a precursor pressure = $9.4 \times 10^{-5}$ Torr. The slope from the linear regression analysis reflects the steady-state growth rate of $ZrO_2$. A positive *x*-intercept indicates an induction period.

the induction period is always less than the day-to-day variability in time required to grow a 2000 Å film of $ZrO_2$. For these reasons, the induction period was neglected in the calculation of the steady-state growth rates.

The linear, steady-state growth rate data (Figure 7a) show that there are three regimes of CVD growth. The first, which is encountered at the lowest deposition temperatures, corresponds to reaction-limited growth. The growth rate is limited by a thermally activated precursor reaction on the ZTB decomposition sequence. At intermediate temperatures (500−675 °C for $9.4 \times 10^{-5}$ Torr and 450−675 °C for $4.4 \times 10^{-5}$ Torr, ZTB), $ZrO_2$ growth is independent of temperature, because the growth rate is limited by precursor flux to the substrate surface. Flux-limited kinetics are clearly indicated by the fact that the deposition rate in this regime approximately doubles when the precursor pressure is increased from $4.4 \times 10^{-5}$ to $9.4 \times 10^{-5}$ Torr. At the highest temperatures, the growth rate decreases with increasing temperature. This type of behavior has often been attributed to precursor depletion due to thermally activated gas-phase precursor reactions. The precursor may be heated through contact with the substrate or hot reactor walls and then collide with other precursor molecules to form particles, which depletes the precursor concentration in the gas phase. While gas-phase precursor depletion has been shown to occur for some precursors under certain conditions, such behavior is unlikely in these experiments because they were performed in a cold-wall reactor at low deposition pressures ($\leq 1 \times 10^{-4}$ Torr).[29−31] Fewer gas molecules become heated and have sufficient thermal energy to react in a cold-wall reactor compared to a hot-wall reactor. The low deposition pressure results in very few molecular

(29) Smith, D.; Alimonda, A. S. *J. Electrochem. Soc.* **1993**, *140*, 1496.
(30) Lux, B.; Colombrier, C.; Altena, H.; Stjernberg, K. *Thin Solid Films* **1986**, *138*, 49.
(31) Dormans, G. J. M.; Meekes, G. J. B. M.; Starring, E. G. J. *J. Cryst. Growth* **1991**, *114*, 364.

collision events due to the large mean free path. As a result, intermediate decomposition events are unlikely.[32]

The growth rate behavior described in this work can be explained using a simple, two-step kinetic model. In the first step, shown in eq 3 below, the precursor (P) reversibly adsorbs on the growing $ZrO_2$ surface. In the second step (eq 4), adsorbed P undergoes an irreversible reaction that ultimately leads to formation of $ZrO_{2(s)}$ and the volatile byproducts ($B_{(g)}$), 2-methylpropene and 2-methyl-2-propanol

$$P_{(g)} \underset{k_{des}}{\overset{k_{ad}}{\rightleftharpoons}} P_{(ad)} \tag{3}$$

$$P_{(ad)} \xrightarrow{k_r} ZrO_{2(s)} + B_{(g)} \tag{4}$$

The parameters $k_{ad}$, $k_{des}$, and $k_r$ are, respectively, the rate constants for precursor adsorption, desorption, and reaction. By analogy to a model developed by us to describe the kinetics of $TiO_2$ deposition from $Ti[OCH(CH_3)_2]_4$ and $Ti(NO_3)_4$, we can write an equation for the steady-state growth rate that would result from the above two-step pathway

$$R = \frac{k_r Z_p S_p^\circ}{(Z_p S_p^\circ/\Theta_p^\circ) + k_{des} + k_r} \tag{5}$$

where $S_p^\circ$ is the zero-coverage adsorption probability of P, $Z_p$ is the gas-surface collision rate, and $\Theta_p^\circ$ is the total number of sites available for precursor adsorption.[13] By allowing for reversible precursor adsorption, eq 5 identifies three limiting cases for CVD growth. Reaction-limited growth occurs at low temperatures when the first term in the denominator is larger than $k_{des} + k_r$, and the growth rate simply becomes equal to $k_r \cdot \Theta_p^\circ$. In this region, the deposition rate is independent of the precursor pressure in the reactor. When $k_r \gg k_{des} + (Z_p S_p^\circ)$, the growth rate is equal to $Z_p \cdot S_p^\circ$. This occurs at intermediate temperatures and makes the growth rate temperature independent. When $k_{des} \gg k_r + (Z_p S_p^\circ)$, the reaction becomes high-temperature limited and now

$$R = \frac{k_r}{k_{des}} Z_p S_p^\circ \tag{6}$$

When the activation energy of desorption is greater than that for reaction, the growth rate will decrease with increasing temperature.

Figure 7b shows the *absolute* growth rate data, which has been fitted to the two-step kinetic model depicted by the solid lines. Linear growth rates (Å·min$^{-1}$) shown in Figure 7a were converted to absolute growth rates (molecules·cm$^{-2}$·s$^{-1}$) using the following procedure: The linear growth rate in Å·min$^{-1}$ was converted to cm·s$^{-1}$ and then multiplied by the temperature-dependent $ZrO_2$ densities shown in Figure 6. A linear interpolation of the two neighboring data points was used to determine the density values of $ZrO_2$ films deposited at temperatures for which no density measurements were made. Finally, the molecular weight of $ZrO_2$ and Avogadro's number were used for the conversion from g·cm$^{-2}$·s$^{-1}$ to molecules·cm$^{-2}$·s$^{-1}$. The absolute growth rate more accurately reflects the amount of material deposited.

**Table 1. Kinetic Parameters Used to Fit the Absolute Growth Rate Data; Parameters Are Defined in the Text**

| parameter | value | parameter | value |
|---|---|---|---|
| $A_r$ | $1.0 \times 10^9$ s$^{-1}$ | $A_{des}$ | $1.0 \times 10^{14}$ s$^{-1}$ |
| $E_r$ | 123 kJ·mol$^{-1}$ | $E_{des}$ | 225 kJ·mol$^{-1}$ |
| $S^\circ$ | 0.0031 | | |

To make the kinetic model fits, $Z_p$ was calculated from gas-kinetic theory, assuming a gas temperature of 25 °C. $\Theta_p^\circ$ was taken as the number density (in cm$^{-2}$) of $ZrO_2$ at the surface of an unreconstructed, monoclinic $ZrO_2$ surface obtained from the density (in g·cm$^{-3}$) for monoclinic $ZrO_2$.[27] All other variables in eq 5 ($A_r$, $E_r$, $A_{des}$, $E_{des}$, and $S_p^\circ$) were used as fitting parameters. The best fit parameters are shown in Table 1; the same set of fitting parameters was used for the two sets of pressure-dependent data. It is important to point out that for this system, true limiting behavior (reaction- or flux-limited) is never obtained. Attempts to extract $A_r$ and $E_r$ from Arrhenius analysis of the low-temperature data failed to yield reasonable values because growth is never entirely reaction limited, even at the lowest deposition temperatures explored in this work. The value obtained for $E_r$ (123 kJ·mol$^{-1}$) is almost identical to the average value reported in other studies (120 kJ·mol$^{-1}$) for ZTB decomposition using an Arrhenius plot at temperatures lower than this study (240−380 °C), where the growth rate was entirely reaction limited.[10] The flux-limited reactive sticking coefficient, $S_p^\circ$, in this study was found to be $3.1 \times 10^{-3}$, which is greater than that reported by Cameron and George ($6.8 \times 10^{-5}$). We cannot offer a reason for this discrepancy.[10]

The two-step kinetic model accurately predicts the growth curves for both ZTB pressures in all three regimes of CVD growth from a single set of fitting parameters. As would be expected by eq 5, at low temperatures the growth rate becomes independent of deposition pressure and both data sets begin to converge. At intermediate temperatures, it is clear that the growth rate is independent of temperature and directly proportional to the deposition pressure. Most importantly, at high deposition pressures, the kinetic model accurately predicts the high-temperature limiting region for both deposition pressures by including the possibility of precursor molecule desorption from the growth surface before reaction. If this high-temperature limiting state were due to gas-phase reactions depleting the precursor in the reactor before it reaches the substrate surface, a lower precursor deposition pressure should reduce this behavior. The experimental data does not show this trend, strengthening the argument that the high-temperature behavior is due to significant precursor desorption.

In the study of Cameron and George, two possibilities were suggested for the observed decrease in deposition rate at high temperature. The first was precursor desorption, which has already been discussed. The second was carbon poisoning of the substrate surface.[10] In the present work, which differs from the nonflow-CVD reactor used by Cameron and George, it does not seem reasonable that ~3 and 5% carbon contamination could be responsible for 34 and 50% drops in the $ZrO_2$

(32) Kodas, T.; Hampden-Smith, M. *The Chemistry of Metal CVD*; VCH: New York, 1994.

growth rate at 743 and 824 °C, respectively, compared to the flux-limited value.

## Conclusion

Zirconium dioxide films were deposited from the metal−organic precursor $Zr[OC(CH_3)]_4$ (ZTB) in a cold-wall, high vacuum CVD reactor. Three kinetic regimes of CVD growth were identified: low temperature (<440 °C) in which the film growth rate is reaction limited, intermediate temperature (440−700 °C) in which the rate is precursor flux limited, and high temperature (>700 °C), in which the rate decreases with increasing deposition temperature. The growth rate measurements were successfully fit to a two-step kinetic model involving reversible precursor adsorption followed by an irreversible reaction step that ultimately leads to $ZrO_2$. The activation energy for precursor desorption exceeds that for the irreversible reaction, which accounts for the high-temperature kinetic regime.

Film microstructure is strongly dependent on deposition temperature and weakly dependent on precursor pressure. Three growth regimes were also identified from microstructure analysis: low temperature (equiaxed $ZrO_2$ grains), intermediate temperature (elongated columnar grains), and high temperature (triangularly shaped grains). Interestingly, the transitions between the different microstructure and kinetic regimes occur at roughly the same temperatures. Similar behavior was reported for $TiO_2$ growth from $Ti[OCH(CH_3)_2]$ and $Ti(NO_3)_4$.[13] Therefore, there appears to be a connection between the molecular-level mechanism for precursor decomposition and the microstructure of the resulting CVD film. This connection will be the subject of future studies.

**Acknowledgment.** This work was supported by the Petroleum Research Fund through PRF-36458-AC5.

CM0107629